

GENERALIZED FEW-SHOT OUT-OF-DISTRIBUTION DETECTION

Pinxuan Li, Bing Cao, Changqing Zhang, Qinghua Hu

College of Intelligence and Computing, Tianjin University

Tianjin Key Lab of Machine Learning

pinxuanli, caobing, zhangchangqing, huqinghua@tju.edu.cn

ABSTRACT

Few-shot Out-of-Distribution (OOD) detection has emerged as a critical research direction in machine learning for practical deployment. Most existing Few-shot OOD detection methods suffer from insufficient generalization capability for the open world. Due to the few-shot learning paradigm, the OOD detection ability is often overfit to the limited training data itself, thus degrading the performance on generalized data and performing inconsistently across different scenarios. To address this challenge, we proposed a Generalized Few-shot OOD Detection (GOOD) framework, which empowers the general knowledge of the OOD detection model with an auxiliary General Knowledge Model (GKM), instead of directly learning from few-shot data. We proceed to reveal the few-shot OOD detection from a generalization perspective and theoretically derive the *Generality-Specificity* balance (GS-balance) for OOD detection, which provably reduces the upper bound of generalization error with a general knowledge model. Accordingly, we propose a Knowledge Dynamic Embedding (KDE) mechanism to adaptively modulate the guidance of general knowledge. KDE dynamically aligns the output distributions of the OOD detection model to the general knowledge model based on the Generalized Belief (G-Belief) of GKM, thereby boosting the GS-balance. Experiments on real-world OOD benchmarks demonstrate our superiority. Codes will be available.

1 INTRODUCTION

Deep learning systems are primarily built upon the theoretical framework of the independent and identically distributed assumption, which presumes identical probability distributions between training and test data. However, real-world data acquisition systems inevitably face challenges of distributional shifts, where such discrepancies in probability distributions may pose significant safety risks, particularly in safety-critical applications such as autonomous driving and medical diagnosis. In response to these challenges, diverse methodologies for OOD evaluation have proliferated. Notably, with the advent of prompt learning in pre-trained vision-language models Radford et al. (2021), CLIP-based prompt tuning Zhou et al. (2022b;a) has been strategically adapted for OOD detection tasks, catalyzing growing research interest in leveraging prompt learning paradigms for enhanced OOD detection capabilities.

Recent advances in few-shot OOD detection leveraging Contrastive Language-Image Pre-training have demonstrated significant progress. Novel few-shot learning methodologies Miyai et al. (2024); Bai et al. (2024); Nie et al. (2024) effectively utilise limited ID data alongside auxiliary OOD samples to enhance model adaptability. However, our experiments reveal a critical limitation of current few-shot learning paradigms for OOD detection - their constrained generalisation capability. Specifically, while these models perform well on specialised OOD datasets, they exhibit substantial performance degradation when evaluated on multi-domain generalised OOD datasets, as demonstrated quantitatively in Fig. 2. This limitation primarily stems from model overfitting to the restricted training distribution, thereby limiting its capacity to recognise diverse unknown OOD patterns in open-world scenarios. One approach to address this challenge is to enhance the diversity of both ID and OOD training samples. However, due to the limitations of the few-shot learning paradigm on real datasets, obtaining large quantities of sufficiently varied OOD samples is unrealistic. Therefore, we propose using a GKM with excellent generalisation capabilities to guide our model. Inspired by this

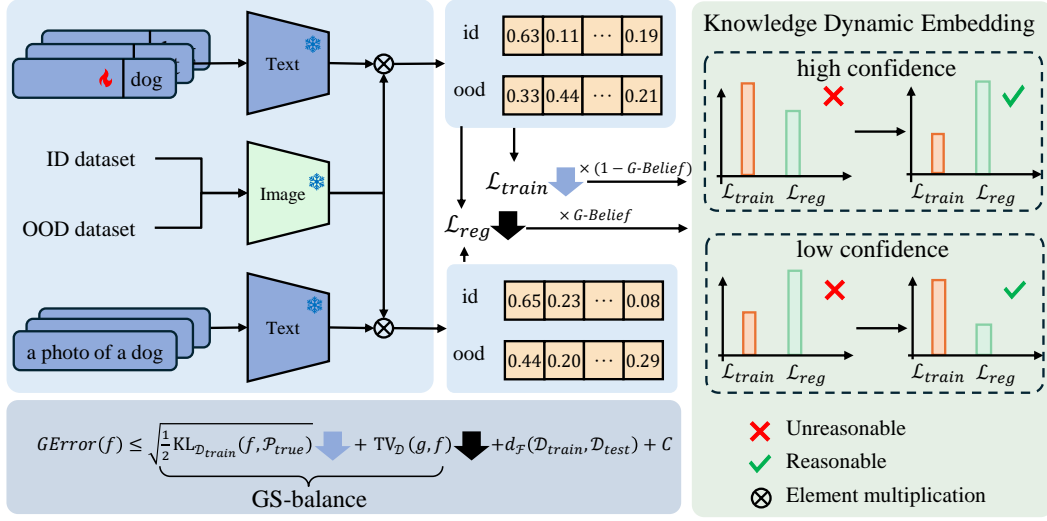


Figure 1: Overview of our framework. Our approach initially introduces a distribution regularization loss aligned with general knowledge. Then, proposed a dynamic credible knowledge learning to explore general knowledge of credible samples, where low-confidence samples allow to explore optimal OOD detection patterns while high-confidence samples preserve reliable general knowledge.

perspective, we propose a theoretical framework that introduces a novel learning paradigm based on GKM.

In this work, we introduce a Generalized Few-shot OOD Detection (GOOD) framework which is illustrated in Fig. 1. First, we reveal few-shot OOD detection from a generalisation perspective, theoretically deriving the *Generality-Specificity Balance* (GS-Balance) for OOD detection. This balance is shown to reduce the upper bound of generalisation error with a general knowledge model. Based on this theoretical foundation, we then propose a distribution regularisation loss between the model outputs and the GKM outputs. This regularisation aims to minimise distributional discrepancies between the trained model and the GKM, thereby preserving the latter’s general knowledge during few-shot learning. Accordingly, we devise a Knowledge Dynamic Embedding (KDE) mechanism to adaptively modulate the guidance of general knowledge. Specifically, based on the GKM’s Generalized Belief (G-Belief), we impose stronger regularisation constraints on samples on which the GKM exhibits high confidence, ensuring the faithful inheritance of reliable general knowledge. Conversely, we relax the regularisation constraints for samples with low confidence, enabling the model to explore optimal OOD detection patterns for uncertain instances. We conduct comprehensive evaluations across diverse OOD benchmarks, including the widely used dataset Huang & Li (2021), the OOD dataset setting from OpenOOD Yang et al. (2022), and the challenging Hard-OOD dataset configured via the MCM protocol Ming et al. (2022). Our method demonstrates effective improvements in both conventional and adversarial OOD scenarios. The contributions of this paper are summarised as follows:

- This paper provides an intuitive and novel Generalized Few-shot OOD Detection paradigm from the perspective of generalization error. Under theoretical analysis, we derive a new Generalized Few-shot OOD Detection (GOOD) framework based on the *Generality-Specificity Balance* (GS-Balance). This offers theoretical guarantees to reduce the upper bound of generalization error in few-shot OOD detection.
- We introduce an auxiliary general knowledge model and propose a Knowledge Dynamic Embedding (KDE) mechanism to adaptively modulate the general knowledge guidance. This offers the generality of the OOD detection model on a specificity basis.
- We developed a Generalized Belief (G-Belief) that provides reliable guidance on general knowledge to avoid potential misguidance from the general model. Experiments validated our theoretical analysis and demonstrated the superior performance of our method.

2 RELATED WORK

OOD Detection with Pre-trained Vision-language Models. Out-of-distribution (OOD) detection aims to identify inputs from unknown classes absent during training, ensuring model reliability. Traditional methods leverage confidence scores like MSP Hendrycks & Gimpel (2016), perturbation-enhanced ODIN Liang et al. (2017), or feature-space metrics such as Mahalanobis distance Lee et al. (2018). Recent advances exploit vision-language models (VLMs) like CLIP, which align visual and textual embeddings for zero-shot inference. Zero-shot CLIP-based approaches Esmaeilpour et al. (2022) utilize pre-trained prompts to estimate OOD score with temperature-scaled softmax to enhance separability without fine-tuning. Beyond zero-shot, fine-tuned methods Du et al. (2022), Tao et al. (2023) incorporate ID data for task-specific calibration, albeit with increased computational costs, such as CLIPN Wang et al. (2023) refine detection via negative prompt generation. Recently, a promising direction is few-shot OOD detection, which balances efficiency and performance by leveraging minimal in-distribution samples. Currently, the mainstream approaches leveraging CLIP-based prompt learning for OOD few-shot detection primarily follow two methodologies. One is the LoCoOP Miyai et al. (2024) method, which enforces entropy uniformity for distribution alignment, and the other adopts a K+1 class formulation that introduces an auxiliary dimension to learn negative prompts. Variants of the latter include techniques such as id-like Bai et al. (2024), which reduces the number of negative prompts by learning common features across categories, and the NegPrompt Li et al. (2024) method, which employs shared class-specific contexts for both positive and negative prompt construction.

Prior knowledge transfer. Prior knowledge transfer has been extensively utilized across various domains. In the context of CLIP, prior knowledge transfer has been widely adopted to address catastrophic forgetting in tasks such as few-shot accuracy prediction and domain generalization. For instance, ProGrad Zhu et al. (2023) ensures alignment between the learning direction of trainable task-specific knowledge and general knowledge (hand-crafted prompts) during prompt tuning, thereby preserving existing knowledge while acquiring new capabilities. Similarly, while ProGrad discards conflicting updates by optimizing prompts toward aligned directions, KgCoOp Yao et al. (2023) avoids knowledge discardment by introducing a Euclidean distance-based loss to constrain trainable task-specific knowledge to remain proximal to general knowledge. Inspired by these approaches, our work investigates catastrophic forgetting in OOD detection and explores how to effectively leverage prior knowledge transfer to enhance OOD detection performance.

3 PRELIMINARIES

We partition the dataset into a training set $\mathcal{D}_{\text{train}} = (\mathcal{D}_{\text{train}}^{\text{ID}}, \mathcal{D}_{\text{train}}^{\text{OOD}})$ and a validation set $\mathcal{D}_{\text{test}} = (\mathcal{D}_{\text{test}}^{\text{ID}}, \mathcal{D}_{\text{test}}^{\text{OOD}})$, where the ID components $\mathcal{D}_{\text{train}}^{\text{ID}}$ and $\mathcal{D}_{\text{test}}^{\text{ID}}$ adhere to the joint data-label distribution (x_i, y_i) with explicit sample-label pairs (x, y) , while the out-of-distribution (OOD) components $\mathcal{D}_{\text{train}}^{\text{OOD}}$ and $\mathcal{D}_{\text{test}}^{\text{OOD}}$ are sampled from unknown P_{OOD} . But current few-shot learning paradigms increasingly avoid reliance on external OOD datasets. Methods exemplified by LoCoOP Miyai et al. (2024) leverage CLIP’s inherent prior knowledge to synthesize OOD samples from ID data through patch-based strategies, while approaches like id-like Bai et al. (2024) generate OOD representations via random cropping of ID samples. Consequently, the majority of OOD data in few-shot scenarios originates from systematic transformations of ID data rather than external collections.

Zero-Shot OOD Detection. Given a pre-trained vision-language model Radford et al. (2021) with image encoder $\phi_I(\cdot)$ and text encoder $\phi_T(\cdot)$. The MCM Ming et al. (2022) method computes OOD scores through cross-modal alignment. MCM’s zero-shot capability stems from leveraging the pre-trained cross-modal alignment without fine-tuning on ID data. The key hypothesis is that OOD samples exhibit lower maximum similarity due to semantic misalignment with ID class prompts. For an input image \mathbf{x} , the scoring function $S(\mathbf{x})$ is defined as:

$$S(\mathbf{x}) = \max_i \frac{\exp(\langle \phi_I(\mathbf{x}), \phi_T(\mathbf{t}_i) \rangle / \tau)}{\sum_{j=1}^C \exp(\langle \phi_I(\mathbf{x}), \phi_T(\mathbf{t}_j) \rangle / \tau)} \quad (1)$$

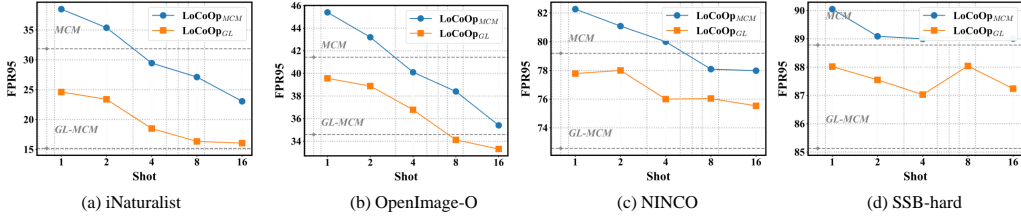


Figure 2: Comparative evaluation across diverse OOD benchmarks, including iNaturalist, OpenOOD-proposed Near-OOD, and MCM-configured Hard-OOD datasets. Our method demonstrates state-of-the-art detection performance, outperforming existing approaches in both few-shot adaptability and boundary case robustness.

where \mathbf{t}_i represents the hand-crafted prompt for class i , and τ is the temperature parameter to be set as 1. The OOD decision rule follows:

$$\mathcal{F}(\mathbf{x}) = \begin{cases} \text{ID}, & S(\mathbf{x}) \geq \tau \\ \text{OOD}, & S(\mathbf{x}) < \tau \end{cases} \quad (2)$$

Prompt learning for OOD detection. In contrast to conventional prompt learning frameworks like CoOp Zhou et al. (2022b), our method adopts the state-of-the-art OOD detection approach LoCoOp Miyai et al. (2024). This framework operates without introducing auxiliary dimensions, instead directly fine-tuning the original classification logit distribution. To address the challenge of detecting real OOD samples under distributional uncertainty, we construct auxiliary OOD data by leveraging low-similarity patches from ID samples under the LoCoOp Miyai et al. (2024) paradigm. A uniform label distribution U is imposed to suppress the original distribution of OOD data. We use C represents the number of ID classes. Our final loss function is formulated as:

$$\mathcal{L}_{train} = \mathcal{L}_{CE} + \lambda \mathcal{L}_{OOD} = \mathbb{E}_{\mathcal{D}_{train}^{ID}} \left[-y_{true} \log f_{true}(x; \theta) \right] + \alpha \mathbb{E}_{\mathcal{D}_{train}^{OOD}} \left[\sum_{i=1}^C \frac{1}{C} \log f_i(x; \theta) \right] \quad (3)$$

Here $f_i(x)$ denotes the predicted probability for class i , λ controls the regularization strength, and C is the number of ID classes.

4 GENERALIZED FEW-SHOT OOD DETECTION

4.1 THEORETICAL FOUNDATIONS OF *Generality-Specificity* BALANCE

Base Setting. Given a dataset \mathcal{D} comprising samples (x, y) , where x includes both ID samples x_{id} and auxiliary OOD samples x_{ood} . The ground-truth distribution \mathcal{P}_{true} corresponds to the true labels for x_{id} or a uniform distribution \mathcal{U} over C classes for x_{ood} .

To formalize the discrepancy between hypotheses, we define the total variation distance (TV) between two hypotheses $f, f' \in \mathcal{F}$ under distribution \mathcal{P} :

$$\text{TV}_{\mathcal{D}}(f, f') = \frac{1}{2} \mathbb{E}_{\mathcal{D}} \left[\sum_{i=1}^C |f_i(x) - f'_i(x)| \right], \quad (4)$$

where $f_i(x)$ and $f'_i(x)$ denote the predicted probabilities for class i by hypotheses f and f' , respectively.

Following Yao Yao et al. (2024), the generalization error of an OOD detector f is defined as:

$$\text{GError}(f) = \text{TV}_{\mathcal{D}}(f, \mathcal{P}_{true}). \quad (5)$$

Note that since our ground-truth distribution \mathcal{P}_{true} corresponds to the true labels for ID samples x_{id} or a uniform distribution \mathcal{U} over C classes for OOD samples x_{ood} , the generalization error defined here inherently measures the joint generalization capability of both ID classification and OOD detection.

We now establish our primary theoretical contribution: an upper bound on the joint generalization error for specificity knowledge and generality knowledge learning balance for OOD detection.

Theorem 1. (*Generality-Specificity balance*) Let g denote a general knowledge model. For any hypothesis $f \in \mathcal{F}$ and $\delta \in (0, 1)$, We holds with a confidence level of $1 - \delta$:

$$GError(f) \leq \underbrace{\sqrt{\frac{1}{2} \text{KL}_{\mathcal{D}_{train}}(f, \mathcal{P}_{true})}}_{\text{Train Loss}} + \underbrace{\text{TV}_{\mathcal{D}}(g, f)}_{\text{Regularization Loss}} + d_{\mathcal{F}}(\mathcal{D}_{train}, \mathcal{D}_{test}) + C \quad (6)$$

where $d_{\mathcal{F}}(\mathcal{D}_{train}, \mathcal{D}_{test}) = \text{TV}_{\mathcal{D}_{test}}(g, f^*) - \text{TV}_{\mathcal{D}_{train}}(g, f^*)$ quantifies the distributional discrepancy between training and test datasets as perceived by the general knowledge model, measured via TV divergence. f^* is the theoretically optimal model. C is constant depending on Rademacher complexities.

The proof is deferred in Appendix A. The generalization error upper bound in our framework is primarily governed by three components: the KL divergence between the training model and groundtruth, the Total Variation distance characterizing the discrepancy between the training model and GKM, and the TV-based distributional shift between training and test datasets as quantified through the lens of the GKM. Where d is a constant determined by the GKM, we refer to the first two items as GS-balance.

Remark1. The KL divergence between the trained model and the ground-truth distribution, along with the TV distance that characterises the deviation of the trained model from the GKM, are pivotal determinants. Integrating the GKM improves the performance of both ID classification and OOD detection. Reducing the upper bound of generalisation errors requires reducing both terms through systematic optimisation. In practice, however, the first and second terms generally contradict each other, so we refer to the sum of the losses of these two terms as the GS-balance.

Remark2. Our theoretical analysis reveals that selecting a well-generalized knowledge model fundamentally governs the parameter $d_{\mathcal{F}}(\mathcal{D}_{train}, \mathcal{D}_{test})$ in the error bound formulation. Such a model, demonstrating superior cross-domain adaptability, exhibits consistent robustness across diverse OOD datasets. This intrinsic generalization capability enables effective quantification of the distributional shift between training and test environments, consequently maintaining relatively lower magnitudes of $d_{\mathcal{F}}$ even when confronted with challenging hard-OOD scenarios.

4.2 KDE:KNOWLEDGE DYNAMIC EMBEDDING

In the preceding section, we established the theoretical foundation for integrating a GKM through derivation of the generalization error upper bound. To minimize the dominant first two terms influencing this bound, we propose the following methodology. Our approach is motivated by the zero-shot CLIP model inherently exhibits superior OOD detection capabilities, as illustrated in Fig. 2. This insight motivates our selection of the zero-shot CLIP as the GKM, upon which we construct a regularization loss that simultaneously minimizes both the model’s training loss and the divergence between its outputs and the knowledge model’s logit distributions. To further refine knowledge guidance, we introduce a Knowledge Dynamic Embedding(KDE). Specifically, this mechanism enforces strong alignment with the generalized knowledge on high-confidence samples while adaptively enhancing OOD discriminative power for low-confidence instances. Such optimization preserves the inherent OOD detection prowess of the zero-shot baseline while enabling progressive adaptation to challenging detection scenarios.

Distribution Regularization Loss. To address our first objective of preventing excessive logit distribution shifts, we note that the zero-shot model inherently exhibits strong OOD detection capabilities across diverse datasets. Motivated by this observation, we introduce a distribution regularization loss to constrain such shifts. As derived in Theorem 1, the upper bound of the generalization error depends on the L1 divergence between the fine-tuned model and the high-performing zero-shot baseline. Consequently, we formalize the distribution regularization loss as the L1 divergence between the logits produced by LoCoOp and those generated by the zero-shot model:

$$\mathcal{L}_{reg} = \frac{1}{C} \sum_{i=1}^C |f_i - f_i^{clip}|$$

where f_i denotes the logit generated by LoCoOp and f_i^{clip} represents the logit produced by the zero-shot model.

Table 1: Benchmark OOD detection performance on ImageNet-1K as the ID dataset across CLIP-based architectures. Results are reported as mean across three randomized seeds. ViT-B/16 is adopted as the reference image encoder.

Method	Backbone	OOD Dataset									
		iNaturalist		SUN		Places		Texture		Average	
		FPR95	AUROC	FPR95	AUROC	FPR95	AUROC	FPR95	AUROC	FPR95	AUROC
		Full/Sub Data Fine-tune									
MSP	CLIP-B/16	40.89	88.63	65.81	81.24	67.90	80.14	64.96	78.16	57.92	82.31
Energy	CLIP-B/16	29.75	94.68	34.28	93.15	56.40	85.60	51.35	88.00	45.83	89.43
ODIN	CLIP-B/16	30.22	94.65	54.04	87.17	55.06	85.54	51.67	87.85	45.65	89.35
Fort/MSP	CLIP-B/16	54.05	87.43	54.12	86.37	72.98	78.03	68.85	79.06	65.29	81.51
VOS	CLIP-B/16	31.65	94.53	43.03	91.92	41.62	90.23	56.67	86.74	43.31	90.50
NPOS	CLIP-B/16	16.58	96.19	43.77	90.44	45.27	89.44	46.12	88.80	35.99	91.48
CLIPN	CLIP-B/16	23.94	95.27	26.17	93.93	33.45	92.28	40.83	90.93	32.74	92.83
		Zero-shot									
MCM	CLIP-B/16	30.91	94.61	37.67	92.56	44.69	89.77	57.77	86.11	44.46	90.16
		One-shot									
CoOp	CLIP-B/16	43.38	91.26	38.53	91.95	46.68	89.09	50.64	87.83	46.90	89.39
id-like	CLIP-B/16	12.07	97.65	40.55	91.07	47.94	88.31	38.34	89.67	34.72	91.67
NegPrompt	CLIP-B/16	65.03	84.56	44.39	89.63	51.31	86.55	87.60	63.76	62.08	81.13
LoCoOp _{MCM}	CLIP-B/16	42.15	91.65	31.95	93.74	38.90	90.93	49.05	89.16	40.54	91.62
LoCoOp _{GL}	CLIP-B/16	28.23	94.51	25.26	94.80	33.63	91.53	51.06	87.39	34.57	91.06
GOOD _{MCM}	CLIP-B/16	28.60	94.10	33.44	93.23	41.57	90.26	49.77	88.84	38.34	91.60
GOOD _{GL}	CLIP-B/16	15.89	96.30	25.42	94.30	34.43	91.20	49.15	86.28	31.22	92.02
		16-shot									
CoOp	CLIP-B/16	35.36	92.60	37.06	92.27	45.38	89.15	43.74	89.68	41.49	90.48
id-like	CLIP-B/16	13.94	95.42	42.28	89.42	53.25	85.44	18.16	93.78	31.91	91.01
NegPrompt	CLIP-B/16	37.79	90.49	32.11	92.25	35.52	91.16	43.93	88.38	37.34	90.57
LoCoOp _{MCM}	CLIP-B/16	21.79	95.77	32.40	93.60	41.43	90.57	41.84	91.01	34.36	92.74
LoCoOp _{GL}	CLIP-B/16	16.88	96.61	23.71	94.93	33.43	91.85	43.54	89.08	29.39	93.12
GOOD _{MCM}	CLIP-B/16	26.16	94.38	31.55	93.37	39.01	90.23	39.22	90.99	33.99	92.24
GOOD _{GL}	CLIP-B/16	17.19	96.09	23.61	94.72	32.77	91.29	41.77	89.41	28.83	92.88

Knowledge Dynamic Embedding. However, the direct incorporation of generic knowledge might introduce erroneous information during the training process. To address this limitation, we propose a dynamic trustworthy learning approach that adaptively leverages reliable knowledge guidance. For high-confidence samples, we enforce consistency with predictions from the zero-shot model to preserve its robust discriminative capabilities. Conversely, for low-confidence samples, we mitigate the influence of general knowledge guidance, enabling the model to enhance its OOD detection performance on these uncertain instances. Based on this idea, we first set the Generalized Belief(G-Belief) as:

$$u = \max_{i \in C} f_i^{\text{clip}} \quad (7)$$

Let u denote the zero-shot model’s confidence score for a sample. The overall loss function of our framework is thus formulated as:

$$\mathbb{E}_{(x,y) \sim \mathcal{D}_{\text{train}}} \left[\mathcal{L}_{\text{train}}(f_i(x; \theta), y) \cdot (1 - u) + \lambda \mathcal{L}_{\text{reg}}(f_i(x; \theta), f_i^{\text{clip}}(x)) \cdot u \right] \quad (8)$$

5 EXPERIMENTS

5.1 EXPERIMENTAL SETUP

Datasets. We evaluate our method across three distinct OOD detection benchmarks to comprehensively assess performance under varying scenarios. First, following standard protocols, we employ ImageNet-1K Deng et al. (2009) as the ID dataset and test on widely-used OOD benchmarks including iNaturalist Van Horn et al. (2018), SUN Xiao et al. (2010), Places Zhou et al. (2018), and Textures Cimpoi et al. (2014) with few-shot training. Second, to rigorously examine hard OOD detection, we adopt the MCM Esmaeilpour et al. (2022) ImageNet-10 and ImageNet-20 setup, where ImageNet-10 mimics CIFAR-10’s class distribution with high-resolution images, and ImageNet-20 introduces semantically similar near-OOD classes. Third, for multi-scale OOD analysis, we follow OpenOOD Yang et al. (2022) Setting. We used ImageNet-1K as the ID dataset, SSB-hard Vaze et al. (2021), NINCO Bitterwolf et al. (2023) and OpenImage-O Wang et al. (2022) as the OOD dataset, evaluating

Table 2: cross-domain OOD detection performance comparison across OOD datasets which under different detection frameworks setting: evaluations follow the OpenOOD benchmark with ImageNet-1K as ID data against SSB-hard, NINCO, and OpenImage-O OOD splits, and the MCM cross-evaluation protocol adopting ImageNet-10 ImageNet-20 as ID datasets with reciprocal OOD testing . Our first row represents the id dataset and the second row represents the ood dataset.

Method	ImageNet-10		ImageNet-20		ImageNet-1K						Average	
	ImageNet-20		ImageNet-10		SSh-hard		NINCO		OpenImage-O			
	FPR95	AUROC	FPR95	AUROC	FPR95	AUROC	FPR95	AUROC	FPR95	AUROC	FPR95	AUROC
MCM	5.60	98.86	11.90	97.68	88.77	64.41	79.24	74.10	41.42	91.84	45.39	85.38
LoCoOp	28.20	92.75	34.40	92.34	90.27	63.16	82.54	69.19	45.12	90.73	56.11	81.63
Ours	5.70	98.60	16.10	97.66	88.78	64.41	79.19	74.10	41.43	91.84	46.24	85.32

robustness against both subtle semantic shifts and domain discrepancies. All results are averaged over three independent trials to ensure statistical reliability.

Implementation details. Our implementation adheres to the LoCoOp framework with CLIP-ViT-B/16 Dosovitskiy et al. (2020) as the backbone, where the feature maps exhibit a spatial resolution of 14×14 . The key hyperparameters are empirically configured as follows: the neighborhood size $K=200$ across all experiments, the knowledge distillation coefficient $\alpha=0.25$, and the regularization weight $\lambda=0.3$. Additional training specifications include 50 epochs with a base learning rate of 0.002, batch size of 32, and prompt token length $N=16$. All experiments are conducted on a single NVIDIA A6000 GPU to ensure hardware consistency.

Baselines and Evaluation. Our comparative analysis encompasses three methodological paradigms. Fully-supervised approaches such as MSP Hendrycks & Gimpel (2016), Fort/MSP Fort et al. (2021), Energy Liu et al. (2020), ODIN Liang et al. (2017), VOS Du et al. (2022), and NPOS Tao et al. (2023), zero-shot approaches represented by MCM Ming et al. (2022), and few-shot methods including CoOp Zhou et al. (2022b) and LoCoOp. All methods employ the CLIP ViT-B-16 backbone to ensure equitable comparison. Performance evaluation leverages three standard metrics — FPR95, AUROC, and ID classification accuracy — to enable comprehensive assessment of detection capabilities.

5.2 MAIN RESULTS

ImageNet-1k as ID dataset. Table 1 summarizes our OOD detection performance using ImageNet-1K as ID data. Our proposed framework, which synergistically integrates CLIP’s intrinsic OOD detection capability with LoCoOp’s adaptive mechanism, achieves state-of-the-art performance across both 1-shot and 16-shot configurations. Particularly noteworthy is the GL-MCM enhanced LoCoOp variant, which demonstrates significant improvements with average FPR95 and AUROC scores of 31.22 and 92.02 in 1-shot settings. This method outperforming conventional OOD detection methods and even surpassing the original zero-shot CLIP baseline and LoCoOp. The framework also notably maintains superior ID classification accuracy, confirming that our loss formulation preserves discriminative power for known classes.

Other large-scale benchmark OOD dataset. To validate cross-dataset generalization, we further evaluate on standard OOD benchmarks set by Openood Yang et al. (2022). As shown in subsequent Table 2, our method consistently matches or exceeds CLIP’s native OOD detection performance without dataset-specific tuning. This empirically validates our key design principle that anchoring adaptation through CLIP’s frozen representations successfully transfers its universal OOD awareness to downstream tasks while circumventing catastrophic forgetting of pre-trained knowledge.

Comparisons on hard OOD detection. Our method demonstrates robust performance on small hard-OOD datasets by maintaining minimal deviation in logit distributions from the zero-shot model, thus preserving its inherent OOD detection capabilities. The result as shown in Table 2. Notably, while LoCoOp suffers significant performance degradation on these datasets, our approach consistently matches or even surpasses the zero-shot baseline, achieving superior OOD detection accuracy. This observation confirms that our framework effectively anchors the optimization trajectory near the zero-shot model’s original solution space, avoiding detrimental shifts toward local optima that compromise generalization on specific OOD distributions.

Table 3: Accuracy comparison of ID on the ImageNet-1K validation data for few-shot object detection.

Shot	Method	Accuracy (%)
1-Shot	CoOp	66.23
	LoCoOp	67.6
	Ours	66.7
16-Shot	CoOp	72.10
	LoCoOp	71.4
	Ours	70.3

Table 4: Ablation analysis of framework components with distribution regularization loss and Knowledge Dynamic Embedding on different OOD datasets with average results.

\mathcal{L}_{reg}	u	OOD Benchmark		Other Benchmark	
		FPR95	AUROC	FPR95	AUROC
✗	✗	40.54	91.62	56.11	81.63
✓	✗	40.33	91.39	45.77	85.46
✓	✓	38.34	91.60	46.24	85.32

5.3 ABLATION STUDY

Importance of distribution regularization loss. As the results are shown in the Table 4. As demonstrated in our ablation studies targeting the two core components of our method – the distributional regularization loss and the confidence-based boundary exploration mechanism – we present aggregated experimental results across benchmark datasets. Our findings reveal that while the proposed distributional regularization loss guarantees superior performance on hard-OOD datasets, its impact remains statistically insignificant on common OOD benchmarks, suggesting this component primarily ensures consistent generalization across diverse OOD test scenarios rather than boosting absolute performance.

Importance of dynamic credible knowledge learning method. Introducing our dynamic credible knowledge learning strategy after the introduction of distributional regularization loss results in a significant performance improvement on the standard OOD evaluation set while maintaining the benefits of cross-distribution generalization. As the results are shown in the Table 4, our approach enables the model to obtain performance improvement on OOD detection, and this performance improvement stems from the fact that we fully utilize the general knowledge guidance of the high-confidence samples and the self-exploratory nature of the unconfident samples, which effectively coordinates the distributional robustness and the discriminative power of the OOD detection task.

Influence of weight of distribution regularization loss. The hyperparameter λ critically governs the distance metric between the text-derived knowledge space and the zero-shot model’s latent representation space. To systematically analyze this relationship, we conduct ablation studies with $\lambda = [0, 0.1, 0.2, 0.3, 0.4, 0.5]$, with comprehensive results visualized in Fig. 3. A particularly noteworthy observation emerges from the $\lambda = 0.1$ configuration, performance degradation occurs due to the induced intermediate embedding space residing in the suboptimal region between the zero-shot prior and LoCoOp’s self-learned representations. This phenomenon suggests that weak regularization fails to achieve effective alignment with either the text-guided semantic structure or the discriminative features autonomously discovered by the model, thereby creating an ambiguous optimization landscape that undermines both knowledge sources’ complementary strengths.

5.4 DISCUSSIONS

The selection of general knowledge model. We propose to select a model with strong generalization capabilities as the general knowledge model to guide our framework. Specifically, We choose the zero-shot model as the general knowledge model for our few-shot task. As demonstrated in Fig. 1 and its superior performance on the different benchmark, the zero-shot baseline outperforms directly trained models like LoCoOp on real-world datasets, exhibiting OOD detection generalizability. This phenomenon underscores the systemic underestimation of zero-shot model intrinsic OOD detection capacity. We think that the performance degradation in LoCoOp may stem from limited training samples inadvertently distorting the zero-shot model’s original output distribution. While minimizing training loss, this training method amplifies the total variation distance between the training model and general knowledge model, thereby degrading generalization across diverse OOD datasets. Theoretically, we argue that selecting an appropriate general knowledge model under principled guidance can effectively tighten the upper bound of generalization error. To validate this claim, we conduct extensive ablation studies in Appendix D, comparing various general knowledge model candidates to verify the effectiveness of our approach.

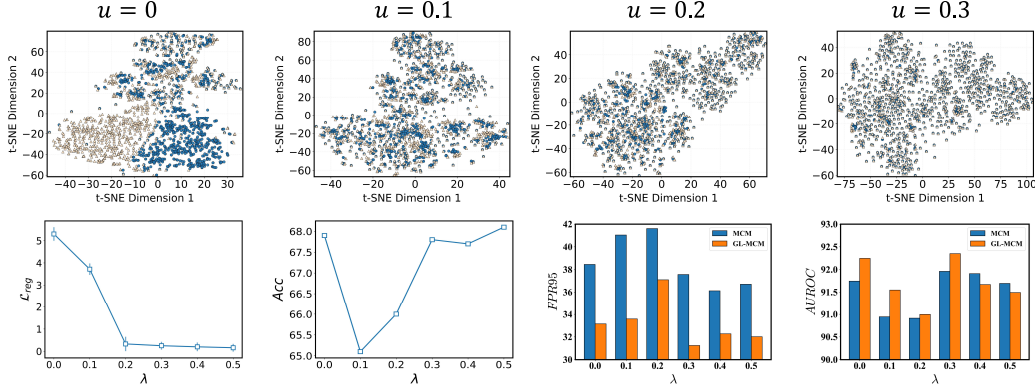


Figure 3: Visualization of latent text space representations and model performance landscapes under varying parameter configurations, demonstrating the alignment between specific trained embeddings (red) and general knowledge distributions (blue), with superimposed performance contours illustrating the rationality of the GS-balance optimization.

The discussion of reusing a prior knowledge. Current few-shot methods, such as LoCoOp and ID-Like, leverage zero-shot as prior knowledge. However, our distinction lies in the application of prior knowledge: their approaches primarily focus on utilizing such priors to partition ID and OOD datasets through image-level operations. This methodology inevitably introduces distributional shifts in the model’s OOD output due to the inherent limitations of finite training data, as exemplified in our experimental results where significant deviation is observed when $\lambda=0$. Consequently, their framework fails to guarantee global optimality on OOD data. In contrast, our method strategically employs prior knowledge in a complementary manner – while existing techniques predominantly operate on the data manifold, our innovation resides in textual space guidance. This orthogonal design principle ensures that our approach remains non-conflicting with LoCoOp’s methodology, as they address different aspects of the few-shot learning paradigm.

The limitations of the exploration scope. The introduction of distribution regularization in our method inherently bounds the exploration of OOD detection performance within the vicinity of the zero-shot model’s distribution. While this constraint ensures stability, it may limit the upper detection bounds on specific datasets. For instance, on the texture dataset, our method—though outperforming the zero-shot baseline—falls short of LoCoOp’s results, as depicted in Table 1. We hypothesize that LoCoOp’s unconstrained exploration in broader parameter spaces could achieve higher OOD detection bounds for such datasets. However, this potential gain risks degrading performance on other OOD benchmarks, including iNaturalist, a trade-off our framework intentionally avoids. We posit that sacrificing marginal gains on niche distributions is a necessary compromise to preserve cross-dataset robustness and prevent catastrophic forgetting of the zero-shot model’s inherent capabilities.

The discussion of generalization errors. The generalization error bound defined in our framework is governed by two loss components. However we observe that there is a partial knowledge conflict between these two losses, as shown in the Fig. 3, there is a balance between our losses, so this is what we call the GS- balance. The derived bound demonstrates an correlation between the magnitude of our proposed loss terms and the tightness of the generalization guarantee. We conduct theoretical analysis in Appendix A to elucidate the relationship between the loss and generalization performance. Our empirical results demonstrate that both the training loss and regularization loss exhibit positive correlations with model performance across diverse OOD datasets, thereby validating the theoretical validity of our framework’s design principles.

6 CONCLUSION

This paper addresses the critical challenge of insufficient generalization in few-shot OOD detection by proposing the Generalized Few-shot OOD Detection (GOOD) framework. Our theoretical analysis reveals that preserving the *Generality-Specificity Balance* (GS-Balance) through general knowledge guidance significantly reduces the upper bound of generalization error. Building on this founda-

tion, we introduced an auxiliary General Knowledge Model (GKM) and developed the Knowledge Dynamic Embedding (KDE) mechanism to dynamically align the OOD detection model with the GKM’s outputs. The proposed Generalized Belief (G-Belief) further ensures reliable knowledge transfer by prioritizing high-confidence guidance from the GKM. Extensive experiments across diverse benchmarks demonstrate that GOOD achieves state-of-the-art performance in both conventional and adversarial OOD scenarios. Future work will explore extending this framework to multi-modal settings and enhancing the GKM’s adaptability for dynamic open-world environments. The integration of uncertainty quantification mechanisms to refine G-Belief estimation also presents a promising research direction.

APPENDIX A PROOF OF THEOREM 1

Following the setup of Zhang et al. (2024), we formally define the Total Variation Distance and Disparity Discrepancy as follows:

Definition 1 (Disparity with Total Variation Distance). *Given two hypotheses $f', f \in \mathcal{F}$. Let \mathcal{D} be a dataset serving as a collection of instances for variable x . we define the Disparity with Total Variation Distance between them as:*

$$\text{TV}_{\mathcal{D}}(f, f') = \frac{1}{2} \mathbb{E}_{\mathcal{D}} \left[\sum_{i=1}^C |f_i(x) - f'_i(x)| \right], \quad (9)$$

Definition 2 (Disparity Discrepancy with Total Variation Distance). *Given a hypothesis space \mathcal{F} and two distributions P, Q , the Disparity Discrepancy with Total Variation Distance is defined as:*

$$d_{\mathcal{F}}(P, Q) := \sup_{f', f \in \mathcal{F}} (\text{TV}_P(f', f) - \text{TV}_Q(f', f)) \quad (10)$$

For any three hypothesis distributions f^1, f^2 and f^3 , the Total Variation Distance satisfies triangle equality, we have

$$\begin{aligned} \text{TV}_D(f^1, f^2) &\leq \text{TV}_D(f^1, f^3) + \text{TV}_D(f^2, f^3), \\ \text{TV}_D(f^1, f^2) &\geq \text{TV}_D(f^1, f^3) - \text{TV}_D(f^2, f^3). \end{aligned} \quad (11)$$

Following YaoYao et al. (2024), the generalization error of an OOD detector f is defined as:

$$\text{GError}(f) = \text{TV}_{\mathcal{D}}(f, \mathcal{P}_{\text{true}}). \quad (12)$$

Where our groundtruth distribution $\mathcal{P}_{\text{true}}$ corresponds to the true labels for ID samples x_{id} or a uniform distribution \mathcal{U} over C classes for OOD samples x_{ood} .

Let f^* be the hypothesis which jointly minimizes the total variance distance between the predicted distribution f^* with uniform distribution \mathcal{U} for OOD data or groundtruth for ID data, which is to say

$$f^* = \underset{f \in \mathcal{F}}{\text{argmin}} \{ \text{TV}_{\mathcal{D}_{\text{train}}}(f, \mathcal{P}_{\text{true}}) + \text{TV}_{\mathcal{D}_{\text{test}}}(f, \mathcal{P}_{\text{true}}) \}. \quad (13)$$

Set $\lambda = \text{TV}_{\mathcal{D}_{\text{train}}}(f^*, \mathcal{P}_{\text{true}}) + \text{TV}_{\mathcal{D}_{\text{test}}}(f^*, \mathcal{P}_{\text{true}})$, then by the triangle equality we have

$$\begin{aligned} \text{GError}(f) &= \text{TV}_{\mathcal{D}_{\text{test}}}(f, \mathcal{P}_{\text{true}}) \\ &\leq \text{TV}_{\mathcal{D}_{\text{test}}}(f, f^*) + \text{TV}_{\mathcal{D}_{\text{test}}}(f^*, \mathcal{P}_{\text{true}}) \\ &= \text{TV}_{\mathcal{D}_{\text{test}}}(f, f^*) + \text{TV}_{\mathcal{D}_{\text{test}}}(f^*, \mathcal{P}_{\text{true}}) + \text{TV}_{\mathcal{D}_{\text{train}}}(f, f^*) - \text{TV}_{\mathcal{D}_{\text{train}}}(f, f^*) \\ &= \text{TV}_{\mathcal{D}_{\text{train}}}(f, f^*) + \text{TV}_{\mathcal{D}_{\text{test}}}(f^*, \mathcal{P}_{\text{true}}) + \text{TV}_{\mathcal{D}_{\text{test}}}(f, f^*) - \text{TV}_{\mathcal{D}_{\text{train}}}(f, f^*) \\ &\leq \text{TV}_{\mathcal{D}_{\text{train}}}(f, \mathcal{P}_{\text{true}}) + \text{TV}_{\mathcal{D}_{\text{train}}}(f^*, \mathcal{P}_{\text{true}}) \\ &\quad + \text{TV}_{\mathcal{D}_{\text{test}}}(f^*, \mathcal{P}_{\text{true}}) + \text{TV}_{\mathcal{D}_{\text{test}}}(f, f^*) - \text{TV}_{\mathcal{D}_{\text{train}}}(f, f^*) \\ &= \text{TV}_{\mathcal{D}_{\text{train}}}(f, \mathcal{P}_{\text{true}}) + \text{TV}_{\mathcal{D}_{\text{test}}}(f, f^*) - \text{TV}_{\mathcal{D}_{\text{train}}}(f, f^*) + \lambda \end{aligned} \quad (14)$$

We have a GKM denfined as $g \in \mathcal{F}$

$$\begin{aligned}
GError(f) &\leq \text{TV}_{\mathcal{D}_{train}}(f, \mathcal{P}_{true}) + \text{TV}_{\mathcal{D}_{test}}(f^*, g) + \text{TV}_{\mathcal{D}_{test}}(g, f) \\
&\quad - \text{TV}_{\mathcal{D}_{train}}(f^*, g) + \text{TV}_{\mathcal{D}_{train}}(g, f) + \lambda \\
&= \text{TV}_{\mathcal{D}_{train}}(f, \mathcal{P}_{true}) + \text{TV}_{\mathcal{D}_{test}}(f^*, g) + \text{TV}_{\mathcal{D}_{test}}(g, f) \\
&= \text{TV}_{\mathcal{D}_{train}}(f, \mathcal{P}_{true}) + \text{TV}_{\mathcal{D}_{train}}(g, f) + \text{TV}_{\mathcal{D}_{test}}(g, f) \\
&\quad + \text{TV}_{\mathcal{D}_{test}}(f^*, g) - \text{TV}_{\mathcal{D}_{train}}(f^*, g) + \lambda
\end{aligned} \tag{15}$$

Due to the inherent limitations in our training data distribution \mathcal{D}_{train} , the discrepancy function $d_{\mathcal{F}}$ fails to achieve the theoretical supremum during empirical risk minimization. Prior work Zhang et al. (2024) hypothesizes that near OOD detection can asymptotically approach zero. In order to circumvent the unachievable condition of supremum, we use a pre-trained foundation model g from large-scale dataset, formally defining the discrepancy function $d_{\mathcal{F}}(\mathcal{D}_{train}, \mathcal{D}_{test})$ as $\text{TV}_{\mathcal{D}_{test}}(f^*, g) - \text{TV}_{\mathcal{D}_{train}}(f^*, g)$. It is evident that this function has become a constant due to the introduction of GKM, which represents the gap between the training set and the test set as perceived by GKM. Consequently, Eq. 15 is expressed as follows:

$$GError(f) \leq \text{TV}_{\mathcal{D}_{train}}(f, \mathcal{P}_{true}) + \text{TV}_{\mathcal{D}}(g, f) + d_{\mathcal{F}}(\mathcal{D}_{train}, \mathcal{D}_{test}) + \lambda \tag{16}$$

Applying Pinsker's Inequality, the following inequality holds

$$\mathcal{L}_{train}(f) \propto KL(f || \mathcal{P}_{true}) \geq 2\text{TV}(F_f(x) || \mathcal{P}_{true})^2 \tag{17}$$

We provide a recap of the Rademacher complexity measure for modelling complexity. We use a complexity-based learning theory to quantify generalisation error. Let \mathcal{D}_{train} be the training dataset. Firstly, we consider the empirical error of f . Then, for $1 > \delta > 0$ there is at least a $1 - \delta$ probability that

$$\begin{aligned}
\text{TV}_{\mathcal{D}_{train}}(f, \mathcal{P}_{true}) &\leq \hat{\text{TV}}_{\mathcal{D}_{train}}(f, \mathcal{P}_{true}) + \mathcal{R}_m(\mathcal{H}) + \sqrt{\frac{\ln(\frac{1}{\delta})}{2M}} \\
&\leq \sqrt{\frac{1}{2}\text{KL}_{\mathcal{D}_{train}}(f, \mathcal{P}_{true})} + \mathcal{R}_m(\mathcal{H}) + \sqrt{\frac{\ln(\frac{1}{\delta})}{2M}}
\end{aligned} \tag{18}$$

where $\hat{\text{TV}}$ is the empirical error of f and $\mathcal{R}_m(\mathcal{H})$ is the Rademacher complexities..

So, We use Eq. 16 and Eq. 18. Finally the generalized error is:

$$GError(f) \leq \underbrace{\sqrt{\frac{1}{2}\text{KL}_{\mathcal{D}_{train}}(f, \mathcal{P}_{true})}}_{\text{Train Loss}} + \underbrace{\text{TV}_{\mathcal{D}}(g, f)}_{\text{Regularization Loss}} + d_{\mathcal{F}}(\mathcal{D}_{train}, \mathcal{D}_{test}) + C \tag{19}$$

where $C = \mathcal{R}_m(\mathcal{H}) + \sqrt{\frac{\ln(\frac{1}{\delta})}{2M}} + \lambda$ represents a constant.

The first item proportional to our train loss, the second item proportional to our regularization loss. As demonstrated in Eq. 17, the initial term is proportional to the model's training loss, while the subsequent term necessitates the restriction of the distance between the logit of our model and GKM on the dataset. Therefore, the second term is to be regarded as the regularization term. In order to guarantee that the regularisation loss can function in such a manner as to reduce the discrepancy between the outputs of the training set and the test set, it is generally necessary to ensure that the fine-tuning methods employed are consistent. One such method that may be employed is the prompt-tuning method, which is selected for both the training set and the test set.

APPENDIX B OOD SCORE

The CLIP model's multimodal feature alignment capability enables the MCM Ming et al. (2022) method to perform zero-shot OOD detection by quantifying the similarity distribution between image features and C class text embeddings. The OOD Score function is defined as follows:

$$S_{MCM} = \max_i \frac{\exp(\langle \phi_I(\mathbf{x}), \phi_T(\mathbf{t}_i) \rangle / \tau)}{\sum_{j=1}^C \exp(\langle \phi_I(\mathbf{x}), \phi_T(\mathbf{t}_j) \rangle / \tau)} \quad (20)$$

where $\tau = 1$ is the temperature parameter, and $\langle \cdot, \cdot \rangle$ denotes cosine similarity.

By introducing a global-local hierarchical feature matching mechanism, GL-MCM Miyai et al. (2025) extends the OOD score calculation to:

$$S_{GL-MCM} = \max_i \frac{\exp(\langle \phi_I(\mathbf{x}^{local}), \phi_T(\mathbf{t}_i) \rangle / \tau)}{\sum_{j=1}^C \exp(\langle \phi_I(\mathbf{x}^{local}), \phi_T(\mathbf{t}_j) \rangle / \tau)} + S_{MCM} \quad (21)$$

where \mathbf{x}^{local} represents the feature of the i -th local image patch.

APPENDIX C EXPERIMENTAL DETAILS

Base OOD Benchmark. The implementation of the system adheres to the LoCoOp framework with CLIP-ViT-B/16 Dosovitskiy et al. (2020), where the feature maps exhibit a spatial resolution of 14x14. The key hyperparameters have been empirically configured as follows: the neighbourhood size $K = 200$ across all experiments, the knowledge distillation coefficient $\alpha = 0.25$, and the regularization weight $\lambda = 0.3$. The additional training specifications encompass 50 epochs with a base learning rate of 0.002, a batch size of 32, and a prompt token length of $N=16$. It is imperative that all experiments are conducted on a single NVIDIA A6000 GPU in order to ensure hardware consistency.

Hard OOD Benchmark. It is evident that our fundamental experimental details are consistent with those of the baseood benchmark. However, given that imagenet-10 and imagenet-20 contain 10 and 20 data types respectively, it was determined that the neighborhood size $K=2$ would be employed for these hard-to-imitate experiments. The results of the model under the 16-shot setting are presented in full in our paper.

OpenOOD OOD Benchmark. The experimental details are fundamentally analogous to the base food benchmark. The imagenet1k has been selected as the ID dataset, while the SSH-hard, NINCO and OpenImage-O have been designated as the OOD dataset. It should be noted that iNaturalist and Texture have not been included in the evaluation process, as these two datasets have previously been evaluated in the base OOD benchmark.

APPENDIX D THE SELECTION OF A SUITABLE GENERAL KNOWLEDGE MODEL

The following experiments are presented, in which other models of general knowledge are selected to guide the model in acquiring general knowledge. The POMP paper Ren et al. (2023) was selected as the secondary general knowledge model to present the experimental results. POMP presented the results of prompt tuning on the ImageNet-21K dataset. In this instance, the model under discussion was employed. It is evident that the parameter settings are consistent with the base OOD benchmark. Our results are shown in Table 5, where the clip subscript represents our general knowledge as "a photo of ", and the POMP subscript represents this general knowledge after training on Imagenet-21k. Our results demonstrate that different GKM models can exhibit varying performance for our method, indicating that our model will acquire distinct general knowledge under distinct GKM settings.

Moreover, in order to demonstrate the rationality of our methodology, we employ the same comparison strategy as outlined in Table 1. The results of the ood score of POMP using MCM and GL-MCM in ood detection are presented, as well as the results of the ood score of the LoCoOp model using only our training loss. The following presentation will outline the output results of the model under the KDE strategy. The results of the study are presented in tabular form. The findings of this study suggest that the proposed methodology explores the upper limit of OOD detection, while exhibiting the POMP generalization.

Table 5: The cross-domain generalisation performance of prompt-tuned general knowledge models, pre-trained on ImageNet-21K and evaluated through out-of-distribution benchmarks.

Method	iNaturalist		SUN		OOD Dataset Places		Texture		Average	
	FPR95	AUROC	FPR95	AUROC	FPR95	AUROC	FPR95	AUROC	FPR95	AUROC
MCM										
GOOD _{CLIP}	27.74	94.16	34.78	93.01	42.55	90.19	48.48	89.05	38.39	91.60
GOOD _{POMP}	30.80	94.17	31.25	93.91	39.78	90.79	41.50	90.81	35.83	92.42
GL-MCM										
GOOD _{CLIP}	13.59	96.81	27.73	93.87	35.94	91.09	51.21	85.80	32.12	91.89
GOOD _{POMP}	16.41	96.48	22.78	95.05	32.41	91.80	44.11	88.95	28.92	93.07

Table 6: The model performance of POMP when used as the GKM model. The present method has been developed in such a manner that it inherits the generalisation ability of POMP, whilst also exploring the upper limit of OOD detection.

Method	iNaturalist		SUN		OOD Dataset Places		Texture		Average	
	FPR95	AUROC	FPR95	AUROC	FPR95	AUROC	FPR95	AUROC	FPR95	AUROC
MCM										
POMP	39.65	92.86	32.44	93.11	39.30	90.73	40.97	90.34	38.09	91.76
LoCoOp	38.96	92.34	32.40	93.60	37.95	91.00	49.32	88.70	39.65	91.41
GOOD	30.80	94.17	31.25	93.91	39.78	90.79	41.50	90.81	35.83	92.42
GL-MCM										
POMP	16.51	96.53	26.12	93.47	33.48	91.14	44.52	86.93	30.15	92.02
LoCoOp	24.38	94.95	25.45	94.77	32.63	91.81	52.32	86.58	33.69	92.03
GOOD	16.41	96.48	22.78	95.05	32.41	91.80	44.11	88.95	28.92	93.07

APPENDIX E MORE EXPERIMENTAL RESULTS

The appendices to this section contain further experimental results of our model, the purpose of which is to demonstrate its experimental performance. The following presentation comprises the experimental results of MCM and GL-MCM under a variety of conditions.

The experimental results obtained under the OpenOOD and MCM benchmarks demonstrate that GL-MCM exhibits superior performance in cross-dataset ID and OOD detection scenarios when compared to the baseline MCM. However, when evaluated within the same dataset containing different class partitions, the method exhibits inconsistent performance, with alternating advantages and disadvantages. It is hypothesised that this discrepancy may stem from the higher similarity of local features between ID and OOD samples originating from the same dataset. The proximity of such inherent features has the potential to diminish the discriminative power of local information, thereby hindering effective ID and OOD separation.

Table 7: OOD detection performance for ImageNet-1k as ID, the SSh-hard, NINCO, OpenImage-O as OOD dataset.

Method	ImageNet-1K					
	SSh-hard		NINCO		OpenImage-O	
	FPR95	AUROC	FPR95	AUROC	FPR95	AUROC
GOOD _{MCM}	88.78	64.41	79.19	74.10	41.43	91.84
GOOD _{GL}	85.13	68.27	72.57	76.06	34.59	92.36

The experimental findings yielded from the execution of MCM benchmarks demonstrate that GL-MCM evinces superior performance in OOD detection scenarios when contrasted with the baseline MCM. This outcome is congruent with our experimental expectations and concomitantly signifies that GL-MCM also attains comparatively favourable enhancement results for GL-MCM of GKM.

The subsequent presentation will expound upon the findings of the model’s image detection process in relation to imaget100, which will be utilised as the ID data. The experimental results of the model on 4-shot are also presented. In the present experiment, the value of K was set to 20. The 1-shot

Table 8: OOD detection performance for ImageNet-10, ImageNet-20 as ID, the corresponding imagenet20, imagenet10 as ood datasets.

Method	ImageNet10 ImageNet20		ImageNet20 ImageNet10	
	FPR95	AUROC	FPR95	AUROC
GOOD _{MCM}	5.70	98.60	16.10	97.66
GOOD _{GL}	10.60	98.66	9.90	98.32

configuration was not selected as the experimental outcome due to the inability of our model to converge on the original LoCoOp setting. In order to conduct a one-shot experiment, it is necessary to enlarge the epoch under the LoCoOp setting until the experimental results obtained are consistent with those reported in the aforementioned paper. The present study employs imagenet-100 as the ID dataset, thereby adopting a methodology that explores enhanced object detection while ensuring the efficacy of the GKM model. This approach is employed to demonstrate the efficacy of the proposed methodology.

Table 9: Cross-domain generalization performance on ImageNet-100 as ID data under four-shot learning protocol. A comparison was made between MCM and LoCoOp.

Method	iNaturalist		SUN		OOD Dataset Places		Texture		Average	
	FPR95	AUROC	FPR95	AUROC	FPR95	AUROC	FPR95	AUROC	FPR95	AUROC
MCM										
MCM	12.58	97.27	32.50	94.93	30.72	94.86	38.33	93.21	28.53	95.07
LoCoOp _{MCM}	18.69	96.54	21.16	96.32	27.82	95.12	26.17	94.99	23.46	95.74
GOOD _{MCM}	10.70	97.71	16.81	96.92	22.52	95.65	24.68	95.49	18.67	96.44
GL-MCM										
GL-MCM	3.17	98.92	17.94	96.85	19.83	96.29	36.20	92.47	19.28	96.13
LoCoOp _{GL}	12.97	97.09	12.55	97.20	18.15	96.06	26.17	94.36	17.46	96.18
GOOD _{GL}	4.44	98.87	13.15	97.42	18.43	96.11	27.23	94.48	15.81	96.72

APPENDIX F GS-BALANCE ANALYSIS

In this section, the relationship between training loss, regularization loss and OOD detection performance is investigated through the lens of GS-balance. In the course of a series of controlled experiments in which regularization coefficients λ were varied, a consistent positive correlation was observed between the total loss values of the models and the OOD detection metrics when the models were sorted by total loss in an ascending order. Moreover, the findings of this study indicate the existence of an inherent discordance between the objectives of optimisation. As demonstrated in Fig. 4, there is a concurrence between the diminution of regularisation loss and the augmentation of training loss. This phenomenon is accompanied by an inverse correlation between these two components. This phenomenon suggests the existence of conflicting knowledge that may hinder concurrent optimisation of both objectives. It is imperative that optimal GS-balance points are identified, at which both losses maintain a mutually beneficial dynamic. The experimental results obtained demonstrate that it is imperative to achieve proper GS-balance through this approach in order to obtain optimal OOD detection performance while maintaining model generalisation capabilities.

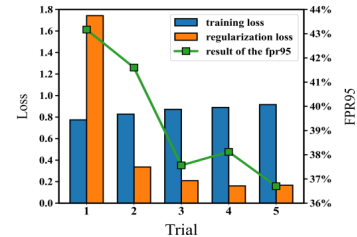


Figure 4: The performance of the training loss and regularisation loss in relation to the OOD detection metric.

APPENDIX G DATASET

APPENDIX G.1 ID DATASETS.

ImageNet-1K. The present study employs the ImageNet-1K benchmark dataset as the ID data source, procured via the official platform (<https://www.image-net.org/>). The experimental design of the present study is aligned with the standardised few-shot evaluation protocol that has been established in CLIP, CoOp and LoCoOp. Model validation is conducted using the ImageNet validation set in its canonical form, which comprises 50,000 annotated images that span 1,000 distinct categories. This configuration is consistent with the evaluation criteria documented in prior research.

APPENDIX G.2 OOD DATASETS.

iNaturalist. The dataset under consideration is comprised of 859,000 biological specimens, which are divided into more than 5,000 taxonomic categories. The primary focus of the dataset is flora and fauna biodiversity. In accordance with the established protocol, the evaluation process is conducted using a sample of 10,000 images, selected at random from a total of 110 classes, with the exclusion of those that are already present in the ImageNet-1K database.

SUN. The scene recognition corpus under consideration contains 130,000 visual instances, which are divided into 397 environmental categories. For the purpose of comparative analysis, a curated subset of 10,000 images has been employed, sampled from 50 ImageNet-disjoint classes.

Places. Places provides complementary coverage of environmental semantics, mirroring SUN’s conceptual scope in scene understanding. The assessment utilises 10,000 images from 50 non-overlapping classes.

TEXTURE. The present corpus is one that has been specifically compiled for the purpose of this study. It consists of 5,640 high-resolution texture patterns that have been organised into 47 material categories. A comprehensive evaluation is performed using the full dataset.

OpenImage-O. This rigorously curated visual recognition benchmark comprises 17,632 images that have been manually filtered through multi-stage quality assurance protocols, achieving 7.8× greater scale diversity than ImageNet-O through pixel-coverage optimisation.

SSB-hard. Derived from ImageNet-21K’s hierarchical ontology through semantic scarcity sampling, this 49,000-image benchmark spans 980 visually complex categories characterised by high inter-class ambiguity.

NINCO. The dataset contains 5,879 meticulously annotated samples across 64 novel categories, thereby introducing conceptual novelty through systematic exclusion of ImageNet-1K semantic overlaps.

ImageNet-10. The creation of ImageNet-10 was driven by the necessity to emulate the class distribution of CIFAR-10, while incorporating high-resolution images. The following categories are contained within the dataset, along with their respective class identifiers: The following subject headings have been identified: The following terms are listed: ‘warplane’ (n04552348), ‘sports car’ (n04285008), ‘brambling bird’ (n01530575), ‘Siamese cat’ (n02123597), ‘antelope’ (n02422699). The following have been identified: ‘Swiss mountain dog’ (n02107574), ‘bull frog’ (n01641577), ‘garbage truck’ (n03417042), ‘horse’ (n02389026), and ‘container ship’ (n03095699).

ImageNet-20. In order to facilitate the evaluation of hard OODs with realistic datasets, ImageNet-20 has been curated. The dataset under consideration consists of 20 classes that are semantically similar to ImageNet-10. The categories are selected based on the distance in the WordNet synsets. The following categories are contained therein: The following items are listed herewith: The following objects are documented: a sailboat (n04147183), a canoe (n02951358), a balloon (n02782093), a tank (n04389033), a missile (n03773504), and a bullet train (n02917067). The following species were documented: A starfish (n02317335), a spotted salamander (n01632458), a common newt (n01630670), a zebra (n01631663), and a frilled lizard (n02391049). For the purposes of this study, the following taxa were selected: the green lizard (n01693334), the African crocodile (n01697457), the Arctic fox (n02120079), the timber wolf (n02114367), the brown bear (n02132136), the moped

(n03785016), the steam locomotive (n04310018), the space shuttle (n04266014) and the snowmobile (n04252077).

APPENDIX H LIMITATIONS AND BROADER IMPACTS

Our framework requires strict consistency in adaptation methodologies between the target model and the GKM. Specifically, both components must employ identical parameter-efficient tuning strategies. Such as the concurrent prompt-tuning of backbone architectures to maintain logit-level alignment. Disparate adaptation approaches such as combining prompt-tuning with conventional backbone fine-tuning disrupt the regularization mechanism’s capacity to minimize train-test output discrepancies, thereby compromising the model’s ability to learn transferable knowledge representations. Moreover, the method under discussion merely provides a means of identifying GS-balance. In the course of the process under discussion, it is possible that more efficacious methods may be discovered for the purpose of ascertaining GS-balance. In conclusion, the methodology employed is founded upon the premise that GKM is a model that demonstrates effective generalisation. The upper limit of the detection of ood explored is constrained by the general knowledge of GKM. The capacity for exploration in the context of prompt-tuning is constrained by this limitation. Alternatively, it may be necessary to compromise certain aspects ood detection capabilities in order to facilitate the generalisation of the model.

REFERENCES

- Yichen Bai, Zongbo Han, Bing Cao, Xiaoheng Jiang, Qinghua Hu, and Changqing Zhang. Id-like prompt learning for few-shot out-of-distribution detection. In *Proceedings of the IEEE/CVF Conference on Computer Vision and Pattern Recognition*, pp. 17480–17489, 2024.
- Julian Bitterwolf, Maximilian Müller, and Matthias Hein. In or out? fixing imagenet out-of-distribution detection evaluation. In *Proceedings of the 40th International Conference on Machine Learning*, pp. 2471–2506, 2023.
- Mircea Cimpoi, Subhansu Maji, Iasonas Kokkinos, Sammy Mohamed, and Andrea Vedaldi. Describing textures in the wild. In *Proceedings of the IEEE conference on computer vision and pattern recognition*, pp. 3606–3613, 2014.
- Jia Deng, Wei Dong, Richard Socher, Li-Jia Li, Kai Li, and Li Fei-Fei. Imagenet: A large-scale hierarchical image database. In *2009 IEEE conference on computer vision and pattern recognition*, pp. 248–255. Ieee, 2009.
- Alexey Dosovitskiy, Lucas Beyer, Alexander Kolesnikov, Dirk Weissenborn, Xiaohua Zhai, Thomas Unterthiner, Mostafa Dehghani, Matthias Minderer, Georg Heigold, Sylvain Gelly, Jakob Uszkoreit, and Neil Houlsby. An image is worth 16x16 words: Transformers for image recognition at scale. *arXiv: Computer Vision and Pattern Recognition, arXiv: Computer Vision and Pattern Recognition*, Oct 2020.
- Xuefeng Du, Zhaoning Wang, Mu Cai, and Yixuan Li. Vos: Learning what you don’t know by virtual outlier synthesis. *arXiv preprint arXiv:2202.01197*, 2022.
- Sepideh Esmaeilpour, Bing Liu, Eric Robertson, and Lei Shu. Zero-shot out-of-distribution detection based on the pre-trained model clip. In *Proceedings of the AAAI conference on artificial intelligence*, volume 36, pp. 6568–6576, 2022.
- Stanislav Fort, Jie Ren, and Balaji Lakshminarayanan. Exploring the limits of out-of-distribution detection. *Neural Information Processing Systems, Neural Information Processing Systems*, Jun 2021.
- Dan Hendrycks and Kevin Gimpel. A baseline for detecting misclassified and out-of-distribution examples in neural networks. *arXiv preprint arXiv:1610.02136*, 2016.
- Rui Huang and Yixuan Li. Mos: Towards scaling out-of-distribution detection for large semantic space. In *2021 IEEE/CVF Conference on Computer Vision and Pattern Recognition (CVPR)*, Jun 2021. doi: 10.1109/cvpr46437.2021.00860. URL <http://dx.doi.org/10.1109/cvpr46437.2021.00860>.

- Kimin Lee, Kibok Lee, Honglak Lee, and Jinwoo Shin. A simple unified framework for detecting out-of-distribution samples and adversarial attacks. *Advances in neural information processing systems*, 31, 2018.
- Tianqi Li, Guansong Pang, Xiao Bai, Wenjun Miao, and Jin Zheng. Learning transferable negative prompts for out-of-distribution detection. In *Proceedings of the IEEE/CVF Conference on Computer Vision and Pattern Recognition*, pp. 17584–17594, 2024.
- Shiyu Liang, Yixuan Li, and Rayadurgam Srikant. Enhancing the reliability of out-of-distribution image detection in neural networks. *arXiv preprint arXiv:1706.02690*, 2017.
- Weitang Liu, Xiaoyun Wang, JohnD. Owens, and Yixuan Li. Energy-based out-of-distribution detection. *Cornell University - arXiv, Cornell University - arXiv*, Oct 2020.
- Yifei Ming, Ziyang Cai, Jiuxiang Gu, Yiyu Sun, Wei Li, and Yixuan Li. Delving into out-of-distribution detection with vision-language representations. *Advances in neural information processing systems*, 35:35087–35102, 2022.
- Atsuyuki Miyai, Qing Yu, Go Irie, and Kiyoharu Aizawa. Locoop: Few-shot out-of-distribution detection via prompt learning. *Advances in Neural Information Processing Systems*, 36, 2024.
- Atsuyuki Miyai, Qing Yu, Go Irie, and Kiyoharu Aizawa. Gl-mcm: Global and local maximum concept matching for zero-shot out-of-distribution detection. *International Journal of Computer Vision*, pp. 1–11, 2025.
- Jun Nie, Yonggang Zhang, Zhen Fang, Tongliang Liu, Bo Han, and Xinmei Tian. Out-of-distribution detection with negative prompts. In *The Twelfth International Conference on Learning Representations*, 2024.
- Alec Radford, JongWook Kim, Chris Hallacy, A. Ramesh, Gabriel Goh, Sandhini Agarwal, Girish Sastry, Askell Amanda, Pamela Mishkin, Jack Clark, Gretchen Krueger, and Ilya Sutskever. Learning transferable visual models from natural language supervision. *Cornell University - arXiv, Cornell University - arXiv*, Feb 2021.
- Shuhuai Ren, Aston Zhang, Yi Zhu, Shuai Zhang, Shuai Zheng, Mu Li, Alexander J Smola, and Xu Sun. Prompt pre-training with twenty-thousand classes for open-vocabulary visual recognition. *Advances in Neural Information Processing Systems*, 36:12569–12588, 2023.
- Leitian Tao, Xuefeng Du, Xiaojin Zhu, and Yixuan Li. Non-parametric outlier synthesis. *arXiv preprint arXiv:2303.02966*, 2023.
- Grant Van Horn, Oisin Mac Aodha, Yang Song, Yin Cui, Chen Sun, Alex Shepard, Hartwig Adam, Pietro Perona, and Serge Belongie. The inaturalist species classification and detection dataset. In *Proceedings of the IEEE conference on computer vision and pattern recognition*, pp. 8769–8778, 2018.
- Sagar Vaze, Kai Han, Andrea Vedaldi, and Andrew Zisserman. Open-set recognition: A good closed-set classifier is all you need. *Learning, Learning*, Oct 2021.
- Haoqi Wang, Zhizhong Li, Litong Feng, and Wayne Zhang. Vim: Out-of-distribution with virtual-logit matching. In *Proceedings of the IEEE/CVF conference on computer vision and pattern recognition*, pp. 4921–4930, 2022.
- Hualiang Wang, Yi Li, Huifeng Yao, and Xiaomeng Li. Clipn for zero-shot ood detection: Teaching clip to say no. In *Proceedings of the IEEE/CVF International Conference on Computer Vision*, pp. 1802–1812, 2023.
- Jianxiong Xiao, James Hays, Krista A. Ehinger, Aude Oliva, and Antonio Torralba. Sun database: Large-scale scene recognition from abbey to zoo. In *2010 IEEE Computer Society Conference on Computer Vision and Pattern Recognition*, Jun 2010. doi: 10.1109/cvpr.2010.5539970. URL <http://dx.doi.org/10.1109/cvpr.2010.5539970>.

- Jingkang Yang, Pengyun Wang, Dejian Zou, Zitang Zhou, Kunyuan Ding, WENXUAN PENG, Haoqi Wang, Guangyao Chen, Bo Li, Yiyu Sun, Xuefeng Du, Kaiyang Zhou, Wayne Zhang, Dan Hendrycks, Yixuan Li, and Ziwei Liu. OpenOOD: Benchmarking generalized out-of-distribution detection. In *Thirty-sixth Conference on Neural Information Processing Systems Datasets and Benchmarks Track*, 2022.
- Haiyun Yao, Zongbo Han, Huazhu Fu, Xi Peng, Qinghua Hu, and Changqing Zhang. Out-of-distribution detection with diversification (provably). *arXiv preprint arXiv:2411.14049*, 2024.
- Hantao Yao, Rui Zhang, and Changsheng Xu. Visual-language prompt tuning with knowledge-guided context optimization. In *Proceedings of the IEEE/CVF conference on computer vision and pattern recognition*, pp. 6757–6767, 2023.
- Qingyang Zhang, Qiuxuan Feng, Joey Tianyi Zhou, Yatao Bian, Qinghua Hu, and Changqing Zhang. The best of both worlds: On the dilemma of out-of-distribution detection. *Advances in Neural Information Processing Systems*, 37:69716–69746, 2024.
- Bolei Zhou, Agata Lapedriza, Aditya Khosla, Aude Oliva, and Antonio Torralba. Places: A 10 million image database for scene recognition. *IEEE Transactions on Pattern Analysis and Machine Intelligence*, pp. 1452–1464, Jun 2018. doi: 10.1109/tpami.2017.2723009. URL <http://dx.doi.org/10.1109/tpami.2017.2723009>.
- Kaiyang Zhou, Jingkang Yang, Chen Change Loy, and Ziwei Liu. Conditional prompt learning for vision-language models. In *Proceedings of the IEEE/CVF conference on computer vision and pattern recognition*, pp. 16816–16825, 2022a.
- Kaiyang Zhou, Jingkang Yang, Chen Change Loy, and Ziwei Liu. Learning to prompt for vision-language models. *International Journal of Computer Vision*, 130(9):2337–2348, 2022b.
- Beier Zhu, Yulei Niu, Yucheng Han, Yue Wu, and Hanwang Zhang. Prompt-aligned gradient for prompt tuning. In *Proceedings of the IEEE/CVF International Conference on Computer Vision*, pp. 15659–15669, 2023.